TESTING MODELS OF THE MOON'S ORIGIN, III: PHASE DIAGRAM OF A PROTO-LUNAR DISK AND CONDENSATION OF TRACE ELEMENTS. M. I. Petaev[1,2] , S. B. Jacobsen[1], S. Huang[3], S. J. Lock[1] and S. T. Stewart[4]. [1]Department of Earth & Planetary Sciences, Harvard University, Cambridge MA 02138; [2]Harvard-Smithsonian CfA, Cambridge MA 02138; [3]Department of Geoscience, University of Nevada, Las Vegas NV 89154; [4]University of California Davis, Department of Earth and Planetary Sciences.

Introduction: The near isotopic identicality between the Earth and Moon accompanied by some chemical differences, especially in volatile elements, implies high-temperature, near-equilibrium processing in a common reservoir which is thought to be a vapor-melt proto-lunar disk formed by the Moon-forming Giant Impact. Recently we reported [1,2] results of physicochemical modeling of evaporation and condensation of the 20 most abundant elements in a proto-lunar disk of different compositions, focusing on a bulk silicate Earth (BSE) bulk composition, for the 10^{-6} – 200 bar pressure range. Here we extend our modeling to a larger number of elements and several isotope systems and discuss implications for a new model of lunar origin [3]. In accompanying abstracts, we use the results for evaluating isotopic fractionations in the proto-lunar disk [4] and core formation in the Moon [5].

Computational technique: Our calculations utilize an extended version of the GRAINS Gibbs energy minimization code [6]. It assumes that a vapor cloud of BSE composition [7], formed after a giant impact, experiences equilibrium condensation upon slow cooling. In addition to full equilibrium, the code can explicitly model the effects of partial condensate isolation (rain-out of droplets) from, or addition of earlier-formed condensates (falling droplets) to, the reactive system in a manner described in [8]. The code also tracks isotopic compositions of O, Mg, Si, K, Ca, Fe, and Zn in the condensed and gaseous phases. The results are compared with a range of available estimates of the bulk Moon composition reviewed in [5].

Instead of the 20 element (H, He, C, N, O, Na, Mg, Al, Si, P, S, Cl, K, Ca, Ti, Cr, Mn, Fe, Co, Ni) version of the code used by [1,2], we updated a 33 element (20 + Cu, Ga, Ge, Mo, Ru, Pd, Hf, W, Re, Os, Ir, Pt, Au) version of the code by adding Zn and expanding the thermodynamic database up to 5000 K. When available (Cu, Ge, Mo, W, Zn), the thermodynamic data for molten and/or solid oxides were added and the latter were used as components of a silicate melt assuming ideal mixing with the major oxides. The earlier extrapolated data for gaseous species [1] were replaced with values taken directly from thermodynamic tables , such as JANAF, or calculated using standard enthalpy of formation, entropy and heat capacity (C_p) polynomials. Also added were several subroutines for calculating condensation along different prescribed P-T profiles (isobaric, adiabatic, isochoric, or an *ad hoc* polynomial). The results reported here were calculated using the ideal silicate melt model and assuming full equilibrium under isobaric conditions.

Results: The calculated equilibrium phase diagram of the proto-lunar disk of BSE composition (Fig. 1) is identical to that of [2] at pressures below 0.1 bar. At higher pressures the melt-vapor curve progressively shifts toward lower temperatures, with the maximum difference reaching ~200 K in the 100 – 200 bars range. This is because the updated data make gaseous species more stable at higher temperatures compared to the extrapolated data. The melt-crystal relationships are not affected by these changes in thermodynamic data. Our new vapor-melt curve is in a reasonable agreement with those of [9,10], although the speciation of the gaseous phase is somewhat different, except for the major species.

Our melt-vapor curve is nearly parallel to the experimental curve of vapor pressure over pure molten silica (pink dashed line in Fig. 1) but shifted toward higher temperatures due to the lower SiO_2 activity (concentration) in the BSE melt. This serves as an indirect validation of our melt-vapor model and implies that the models of proto-lunar disk based on the EOS for pure SiO_2 significantly underestimate the melt-vapor ratios in such a disk. Despite significant deviation at lower pressures, the melt-vapor curve for ANEOS dunite (purple dotted line in Fig. 1) employed by [3], is very close to our curve in the ~20 – 200 bars pressure range, implying a good consistency between the physical [3], chemical and isotopic [4] models of the proto-lunar disk.

Among three different isobaric condensation (and re-evaporation) sequences described in [2], at least two are applicable to the new model of the proto-lunar disk [3]. At the pressure range of $\sim 10^{-5} - 2\times10^{-3}$ bar, representing the exosphere of the proto-lunar disk, the initially condensed Ca,Al,Ti-rich and SiO_2-poor melt rapidly solidifies into a mixture of corundum, Ca-olivine and spinel that upon further reaction with the ambient vapor transforms into an olivine-melt mixture that solidifies at 1850 K.

At higher pressures, cooling vapor of BSE composition would condense as a silicate melt of nearly BSE composition (except for the volatiles), with the condensation rate slowing down with falling pressure as indicated by the vapor isopleths in Fig. 2. Cooling below ~2540 K (Fig. 1) results in the crystallization of

periclase followed by Ca-olivine (s10% isopleth) with the combined crystal content rising to ~ 30 wt%; both phases react with the melt at ~2100 K to form forsterite (s75% isopleth). Finally, the melt solidifies at 1850 K as a mixture of olivine, plagioclase, ortho- and clinopyroxene containing ~1 wt% of partially molten Fe,Ni metal which first segregates from the silicate melt in the 2700 – 3100 K temperature range (pressure dependent).

Pressure also affects the condensation sequence of some minor (Cr, K, Na) and trace (Cu, Zn, Ge, Mo) elements making the elemental patterns a sensitive indicator of the P-T conditions of lunar formation.

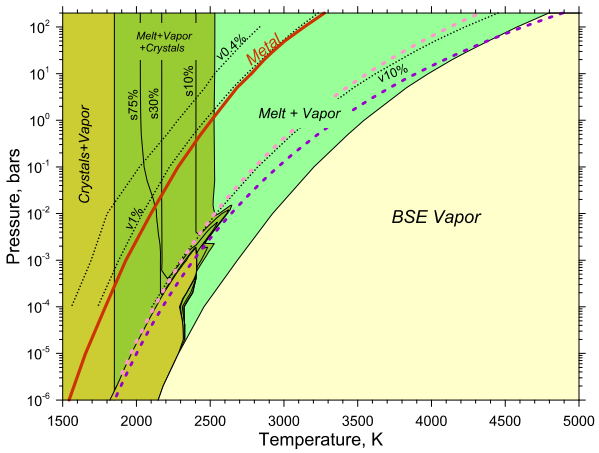

Fig. 1. Phase diagram of the proto-lunar disk of BSE composition. The heavy red line shows the onset of metal segregation from the homogeneous silicate melt. Dotted lines (labeled v#%) show vapor contents in wt%. Solid lines (labeled s#%) are isopleths of crystal contents in wt%. The dashed pink and purple lines show the vapor pressure over pure molten silica [11] and the vapor-melt curve for ANEOS dunite used by [3], respectively.

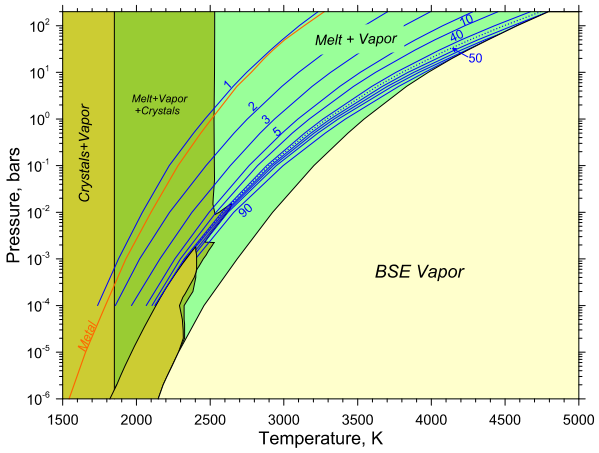

Fig. 2. Vapor isopleths (blue lines) in wt%. Note the narrow temperature range for substantial condensation/evaporation of BSE melt at high pressures (in the Melt+Vapor field).

Implications for the Moon's origin: Our calculations indicate that metal droplets will precipitate from an initially homogeneous silicate melt in the molten Moon as it cools. As a result, we expect an identical W isotopic composition of the Moon and Earth [5]. Our work addresses the range of possible pressure and temperatures of lunar origin by predicting the elemental patterns of BSE condensate, as shown in Fig. 3. Overall, the major element pattern of the Moon can be reproduced by equilibration between the silicate melt and ambient vapor in the system of BSE composition at any pressure. However, minor and trace element depletions argue against both low (Cu, Zn, Ge, Na) and high (Cu) pressures. The most reasonable fits to the estimated bulk composition of the Moon are calculated for the pressure range of ~15-25 bars. Our empirical best fits for the equilibrium pressures and temperatures of lunar origin are in excellent agreement with the predicted pressures and temperatures of equilibration between the Moon and the BSE in a new physical model for lunar accretion [3].

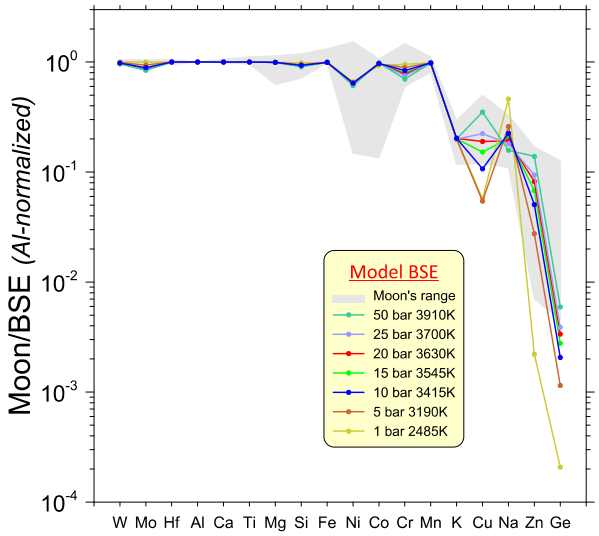

Fig. 3. BSE and Al-normalized model compositions of the Moon calculated at different P-T conditions (see legend). At each pressure, the temperature of the best fit was chosen based on the K depletion factor of 0.2. At these temperatures ~8-10 at% Si still remains in the gaseous phase.

References: [1] Petaev M.I. et al. (2014) *LPS* **45**, Abstract #2316. [2] Petaev M.I. et al. (2015) *LPS* **46**, Abstract #2254. [3] Lock S.J. et al. (2016) *this volume.* [4] Huang S. et al. (2016) *this volume.* [5] Jacobsen S. B. et al. (2016) *this volume*. [6] Petaev M. I. (2009) *CALPHAD, 33*, 317-327. [7] McDonough W.F. and Sun S.S. (1995) *Chem. Geol.* **120**, 223-253. [8] Petaev M.I. and Wood J.A. (1998) *MAPS* **33**, 1123-1137. 5934. [9] Visscher C. and Fegley Jr., B. (2013) *ApJ* **767**, 1-6. [10] Schaeffer L. et al. (2012) *ApJ* **755**, 41. [11] Ward W.R. (2012) *ApJ* **744**, 140-150.